Spin-dependent transport across anti-phase boundaries in magnetite films

Eerenstein, Willemina

Chapter 7

Magneto-Resistance in epitaxial Fe_3O_4 films

7.1 Introduction

Spin-polarised transport phenomena have received increasing attention over the past years. A prominent example is the large magneto-resistance (MR) effects observed in magnetic multilayers [117] used in magnetic field sensors like read heads [31]. Despite its technological importance, the MR me-chanism in these so-called spin-valves is not well understood, because it is difficult to discriminate between the many factors that influence the MR, such as band structure, magnetic impurities, structural disorder and interface roughness [32, 33].
In this chapter we introduce a new and simpler type of spin-valve system. It consists of two ferromagnetic domains coupled anti-ferromagnetically at an atomically sharp interface. In case of spin-polarised conduction electrons and assuming that spin-dependent scattering does not occur at the interface, electron transport is completely blocked. The current can be turned on by a magnetic field, because it will tilt the anti-parallel spins. Note, that the MR of such a system is infinitely large.
This spin-valve mechanism is in fact realized in magnetite (Fe_3O_4) layers grown epitaxially on MgO substrates. We assume that the conduction electrons are fully spin-polarised (sp), which follows from band calculations which show that magnetite is a half-metallic ferrimagnet with a gap at the Fermi energy for the spin up, but not for the spin down electrons [2, 3]. Recent spin-polarised photo-emission experiments support this view, as further

---

The main results of this chapter have been published in:
W. Eerenstein, T.T.M. Palstra, S.S. Saxena and T. Hibma Phys. Rev. Lett. **88**, 247204 (2002), and in:
W. Eerenstein, T.T.M. Palstra and T. Hibma, Thin Solid Films **400**, 90 (2001).

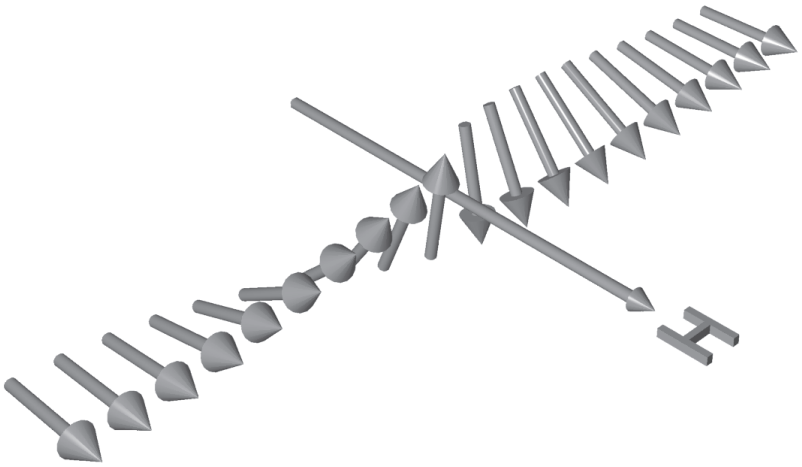

Figure 7.1: *Spin-Orientation of two ferromagnetic chains with anti-ferromagnetic coupling at an atomically sharp boundary subject to a magnetic field.*

explained in §2.6. In §2.3 we explained that anti-phase domain boundaries (APB) are present in epitaxial Fe_3O_4 films [23, 24, 36]. The APB are natural growth defects, resulting from the fact that the lattice constant of Fe_3O_4 (a = 8.3987 $\AA$) is twice as large as the one of MgO (a = 4.212 $\AA$). The magnetic coupling over a large fraction of these boundaries is anti-ferromagnetic (AF), see also chapter 5. The spin-polarised electrons encounter a high resistance at the AF-APB. Upon application of a magnetic field, the AF spins will align themselves to some degree with the magnetic field, thus increasing the electron transport across the boundaries. This is shown schematically in Fig. 7.1.

7.2 Experimental

We have investigated the magneto-resistance effects for ultrathin epitaxial Fe_3O_4 films by means of resistance measurements in fields up to 5 Tesla with the field both parallel and perpendicular to the film plane. The Fe_3O_4 ultrathin films (12 and 40 nm thick) were grown on MgO (001) substrates using Molecular Beam Epitaxy (MBE). During growth an oxygen pressure of 10^{-6} mbar, a substrate temperature of 250 °C and an iron flux of 1.2 $\AA$/minute were used, this procedure is known to give a good stoichiometry [24]. Resistance measurements were performed in a commercial PPMS system from Quantum Design (contacts consisting of 20 nm Ti and 40 nm Au). Linear I/V curves were obtained by applying dc voltages and measuring the current in a four-point geometry along the [100] direction of the films. Structural investigation of the films was done with transmission

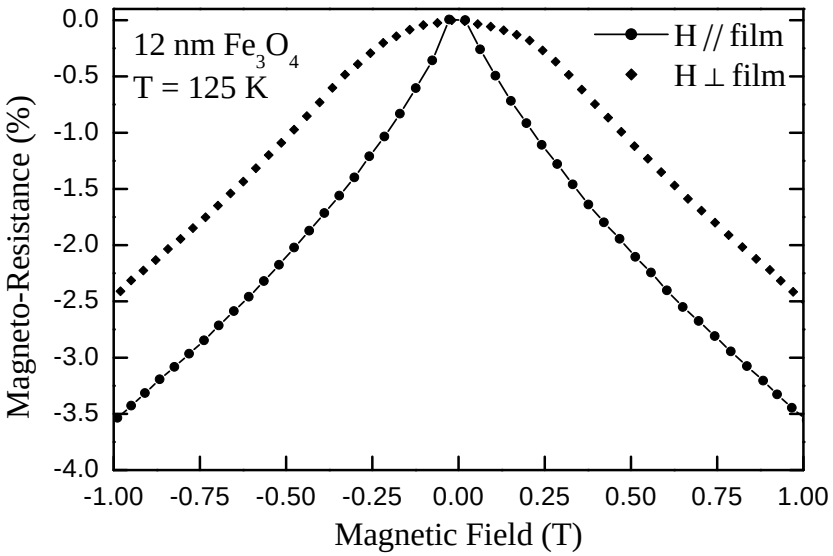

Figure 7.2: *Low field magneto-resistance of 12 nm thick epitaxial Fe_3O_4 films at 125 K for magnetic fields applied perpendicular and parallel to the film. Up to 0.5 Tesla, the out of plane field dependence is quadratic, whereas the in plane field dependence is linear*

electron microscopy (TEM) on a JEOL 2000FX microscope operating at 200 keV. TEM specimens were prepared by floating the Fe_3O_4 films off the MgO substrate in a 4 wt.% ammonium sulphate solution at 70 °C. Dark field images were obtained with the spinel (220) reflection.

7.3 Spin-polarised transport across sharp AF boundaries

Fig. 7.2 shows low field MR measurements (up to 1 Tesla) on the 12 nm thick sample measured at 125 K, with the magnetic field applied both perpendicular and parallel to the film plane. The out-of-plane MR measurements show quadratic behaviour up to 0.5 T, whereas the in-plane MR behaviour is linear in this regime. In this paragraph we will demonstrate that these results are consistent with a model of spin-polarised transport across an atomically sharp anti-ferromagnetically coupled boundary between two ferromagnetic chains.

7.3.1 Spin-polarised transport across a single boundary

As explained in §2.4, the electron transport occurs through small polaron hopping [22, 21] and the conductivity is proportional to the square of the

hopping integral t, i.e.: σt^2. If the spin on a neighboring ion is rotated over an angle φ_{nn}, the transfer integral is reduced to $t = t_0 \cos\varphi_{nn}/2$. Consequently, the transfer of the conduction electron between ions with anti-parallel spins at an AF-APB is blocked and the conductivity is zero. On application of a magnetic field, this angle deviates from π and the conductivity becomes finite.
The magnetic field (H) dependence of the conductivity (σ) will now be calculated in a 1-dimensional model by considering a chain of spins coupled ferromagneticly with one anti-ferromagnetic boundary. A magnetic field aligns the spins far from the boundary, whereas the spins close to the boundary are only slightly affected by the field, as shown in Fig. 7.1.
At weak fields the configuration can be affected by magnetic anisotropies. We only take the uniaxial anisotropy into account since in magnetite films the magnetocrystalline anisotropies are of minor importance [115, 119].

Magnetic field parallel to the film plane

For magnetic fields parallel to the film most of the spins remain in the plane of the film so that the uniaxial anisotropy term does not play a role. We will start the calculation by considering only a half-infinite spin chain, i.e. a spin chain on one side of the anti-ferromagnetic boundary. The energy per unit area of such a chain, γ_1 is given by [118]:

$$\gamma_1 = \int_{-\infty}^{0} \left(-M_s H \cos\varphi + A_F \left(\frac{d\varphi}{dx} \right)^2 \right) dx \tag{7.1}$$

The first term in the integral is the Zeeman and the second term the nearest neighbour exchange contribution. The angle between the saturation magnetization M_s and the magnetic field H is φ, and A_F is the exchange stiffness constant. Following standard variational calculus procedures, the second or integrated Euler condition can be written as

$$-M_s H(\cos\varphi - \cos\varphi_{-\infty}) = A_F \left(\frac{d\varphi}{dx} \right)^2 \tag{7.2}$$

Since the spins far from the boundary are parallel to each other and to the field, $\cos\varphi_{-\infty} = 1$. It is now straightforward to calculate the equilibrium configuration of the half-infinite spin chain and the total energy from equations 7.1 and 7.2 for a given value of φ.
Next we will determine the equilibrium configuration of the full chain. This is done by minimising the total energy of the full chain, consisting of the contribution γ_1 and γ_2 of two half infinite chains on either side of the boundary and an anti-ferromagnetic coupling energy at the boundary [118]

$$\gamma_{total} = \gamma_1 + \gamma_2 + \frac{A_{AF}}{d} \left[1 - \cos(\varphi_2 - \varphi_1) \right] \tag{7.3}$$

where φ_1 and φ_2 are the angles between the spins at the left- and right hand side of the boundary and the magnetic field respectively. A_{AF} is the (negative) exchange stiffness constant for the AF exchange interaction at the boundary and d is the distance between two neighboring spin chains along the boundary. The total energy has to be minimized with respect to φ_1 and φ_2. The derivatives of the energy for the half-infinite chains can be calculated using the relation $d\gamma/d\varphi = 2A(d\varphi/dx)$, which can be derived from eq's (1) and (2). The final result of the minimization is: $\varphi_1 = -\varphi_2 = \varphi_{nn}/2 = \varphi_{AF}$ and

$$HM_s = W_{AF}\left(\cos^2\varphi_{AF} + \cos^3\varphi_{AF}\right) \tag{7.4}$$

where $W_{AF} = A_{AF}^2/A_F d^2$. Taking the literature values for A_F and the anti-ferromagnetic coupling in magnetite [23, 24], in a field of 1 Tesla $W_{AF}/HM_s \geq 10$. For such a strong AF coupling the angle φ_{AF} will still be close to $\pi/2$, and the cubic term may be neglected, and we obtain:

$$\cos^2\varphi_{AF} = \frac{HM_s}{W_{AF}} \tag{7.5}$$

In order to calculate the conductivity we recall that $\sigma \propto t^2 = t_0^2\cos^2\varphi_{AF}$. As long as the alignment at the boundary is nearly anti-parallel, by far the largest mobility drop will be experienced at the interface. Based on equation 7.5 we expect that the transport through an AF-APB without magnetic anisotropy is blocked if no magnetic field is present, and increases approximately linearly with a magnetic field.

Magnetic field perpendicular to the film plane

If a weak field is applied perpendicular to the plane of the film, the uniaxial anisotropy has to be taken into account. Adding the uniaxial anisotropy energy density $K\cos^2\varphi$ to the integral of equation 7.1 two different regimes can be distinguished for the field dependence. For external magnetic fields smaller or larger than the uniaxial anisotropy field H_{an} the following approximate results are obtained:

$$I : H < H_{an} \rightarrow \cos^2\varphi = \frac{(M_s H)^2}{4KW_{AF}} \tag{7.6}$$

$$II : H > H_{an} \rightarrow \cos^2\varphi = \frac{M_s H - K}{W_{AF}} \tag{7.7}$$

Following the argument used previously, we expect that the conductivity of an AF-APB changes quadratically with a magnetic field along a hard magnetization axis until it equals the anisotropy field, and is approximately linear for higher fields.

7.3.2 Spin-polarised transport across many AF-boundaries

The magneto-resistance measurements were performed on ultrathin layers of magnetite containing many AF-APB. Transmission electron microscopy (TEM) analysis shows that the average domain size for a 12.5 nm and a 40 nm thick film are 30 and 50 nm respectively. More details on the domain sizes can be found in chapter 4. The total conductivity of such samples is then a function of the bulk conductivity σ_b and of the boundary conductivity σ_{APB} and also depends on the APB density. The fraction of both bulk and boundary material, ϕ_b and ϕ_{APB}, relate as $\phi_b + \phi_{APB} = 1$. The domain size increases significantly with increasing film thickness [114], leading to an increase in ϕ_b. Domain sizes and values for ϕ_b for various film thicknesses are tabulated in table 7.1. As explained in chapter 6, this also results in an increase in conductivity and using the effective medium approximation we obtained for the total conductivity [114]:

$$\begin{aligned} \sigma_e &= 0.5 * [(\sigma_b - \sigma_{AF})(2\phi_b - 1) + \\ &\quad \sqrt{(\sigma_b^2 + \sigma_{AF}^2)(2\phi_b - 1)^2 + 2\sigma_b\sigma_{AF}(2 - (2\phi_b - 1)^2)}] \end{aligned} \tag{7.8}$$

The magneto-resistance is defined as

$$MR = \frac{\rho_H - \rho_0}{\rho_H} \tag{7.9}$$

and can be calculated by inserting Eqn. 7.8. In zero magnetic field, the boundary conductivity will be much lower then the bulk conductivity and can be neglected. The total *zero-field* conductivity for samples with a bulk fraction larger then 0.5 can be approximated as[114]:

$$\sigma_e = \sigma_b(2\phi_b - 1) \tag{7.10}$$

In that case we obtain for the magneto-resistance:

$$\begin{aligned} MR &= -\frac{\sigma_{AF}}{\sigma_b}\left(\frac{1}{(2\phi_b - 1)^2} - 0.5\right) \\ &= -cos^2\varphi_{AF}C \end{aligned} \tag{7.11}$$

where C is: $\frac{1}{(2\phi_b-1)^2} - 0.5$ and the values of C for the different film thicknesses are also given in table 7.1. The value of C, and therefore the magneto-resistance, depends on the fraction of bulk material and thus on the film thickness.
For magnetic field applied parallel to the film plane, $\cos^2\varphi_{AF}$ is given in Eqn. 7.5 and the magneto-resistance can then be written as:

$$MR = -\frac{HM_s}{W_{AF}}C \tag{7.12}$$

Table 7.1: *Structural domain size, RT conductivity, volume fraction of bulk phase and magneto-resistance for different film thicknesses of Fe_3O_4 films on MgO*

Film thickness (nm)	Domain Size (nm)	Conductivity $((\Omega cm)^{-1})$	ϕ_b	MR// (H = 5 T) (%)	M_s/W_{AF} (1/T)
12	11	58.8	0.67	-3.27	$8.5{\cdot}10^{-4}$
25	20	119	0.81	-2.81	$3.5{\cdot}10^{-3}$
50	28	189	0.86	-2.20	$4.8{\cdot}10^{-}$
100	40	192	0.90	-2.02	$7.2{\cdot}10^{-3}$

from which the ratio M_s/W_{AF} can be calculated.
The experimental value for the room temperature magneto-resistance in a parallel applied field of 5 Tesla and the corresponding values for M_s/W_{AF} are given in table 7.1. Inserting the bulk value for the magnetisation into the obtained ratio of M_s/W_{AF} enables one to calculate W_{AF}. Because $W_{AF} = A_{AF}^2/A_F d^2$, a value for the anti-ferromagnetic coupling strength can be obtained. The obtained value of 20 K is in good agreement with the estimated value of 25 K. The value of 20 K has been obtained assuming 2 anti-ferromagnetic interactions per unit cell.
The model can be applied to describe the shape of the magneto-resistance curves. Eqn. 7.11 shows that even for a sample containing many AF-APBs, the magneto-resistance is proportional to the average (negative) single boundary conductivity.
The model gives a good qualitative description for the observed features of the MR behaviour. Fig. 7.2 shows that the low in-plane field behaviour of the MR curve is linear in the applied field, as expected from equation 7.5. This figure also shows that for the out-of-plane measurements the MR has a quadratic field dependence for fields smaller than 0.5 T. This value is in good agreement with the uniaxial anisotropy field of 0.53 T obtained from magnetization loops for a 115 nm thick Fe_3O_4 film [119]. The MR for magnetic fields below the anisotropy field, applied perpendicular to the film plane, is thus accurately described by equation 7.6.
For larger fields, a linear dependence on the magnetic field is expected. The full field MR behaviour (up to 5 Tesla) for 12 and 40 nm thick films measured at 125 K (magnetic field applied both parallel and perpendicular to the film plane) is shown in Fig. 7.3. The high field behaviour starts to deviate from linearity. These deviations can partly be explained by taking the full field dependence of Eqn 7.5 into account. For larger fields, the cubic term in Eqn 7.5 can not be neglected (as in 5 Tesla $W_{AF}/HM_s \geq 2$) and causes the MR to deviate from linearity. Another contribution to the non-linearity is the distribution of AF exchange coupling strengths for the

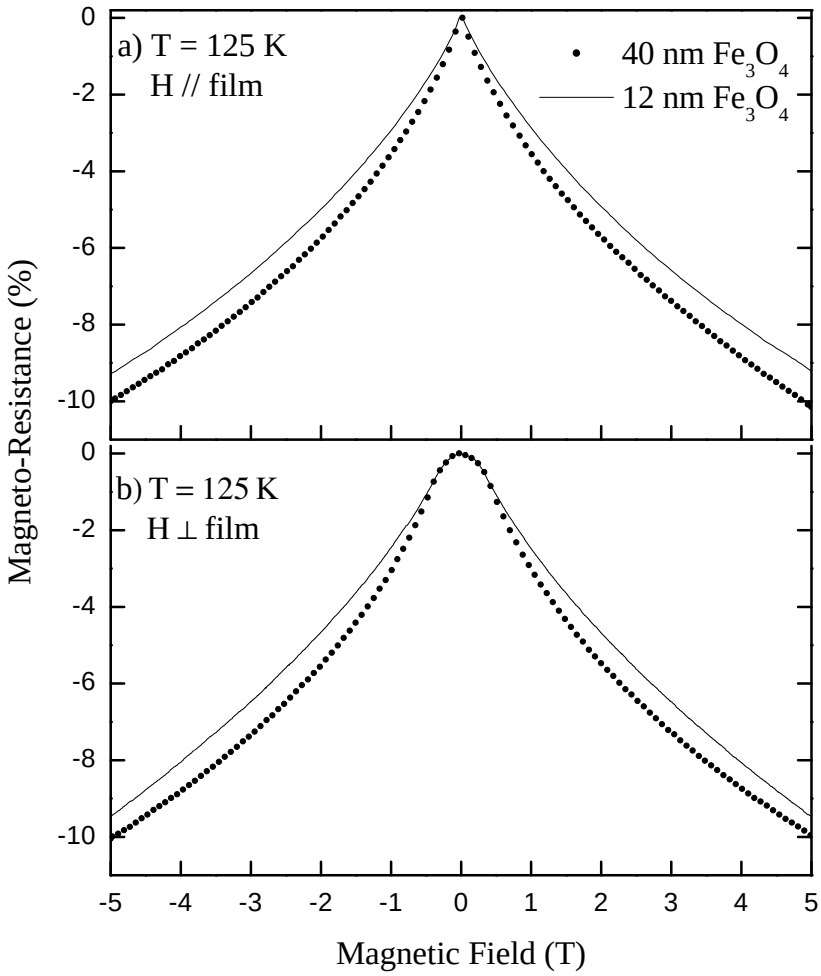

Figure 7.3: *High field magneto-resistance of 12 and 40 nm thick epitaxial Fe_3O_4 films at 125 K for magnetic fields applied a) parallel to the film and b) perpendicular to the film.*

boundary regions. This results from the fact that different types of boundaries [23] do not have the same number of AF coupled neighbors in the boundary region. In regions where more than 2 boundaries meet, the AF coupling might be frustrated [24] which also changes the effective AF coupling strength. The MR decreases with increasing temperature. At 300 K, the MR is reduced to 3 percent (not shown here). However, the shape of the MR curves is independent of temperature. This is shown in Fig. 7.4, where the curves have been normalized by taking the value at 5 Tesla to be -1. This observation is in excellent agreement with the model presented above since the field dependent part of the conductivity is a single boundary property and does not depend on temperature. Even though the equation for the magneto-resistance does not contain any temperature dependent terms,

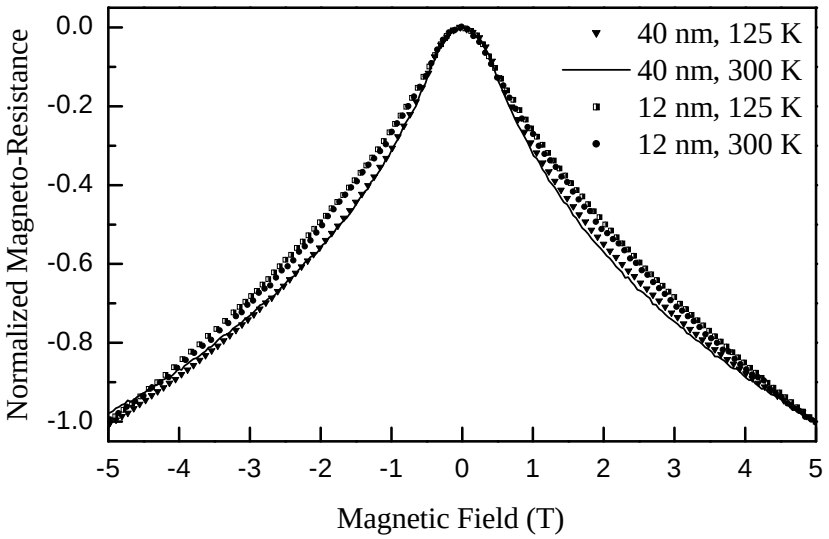

Figure 7.4: *Normalized magneto-resistance (at 125 and 300 K) by taking the value at 5 Tesla to be -1, for 12 and 40 nm thick epitaxial Fe_3O_4 films and magnetic fields applied perpendicular to the film. The shape is independent of temperature, but depends on the film thickness*

it should be noted that the spin-polarisation is temperature dependent and also has an influence on the magneto-resistance. Furthermore, the equation for the total conductivity, Eqn. 7.8 is not valid below T_v, as explained in §6.5.
The shape does change with film thickness, which is reflected in the fact that M_s/W_{AF} is thickness dependent. M_s is however not always equal to the bulk value, but decreases with decreasing film thickness [125].
Figs. 7.3 and 7.4 both show that the MR curves are still not saturated in applied fields of 5 Tesla. Margulies *et al.* [23] observed that the same holds for the magnetization, which has not saturated in applied fields of 7 Tesla. This has also been related to the strong anti-ferromagnetic exchange coupling at the APB.

7.4 Discussion of the magneto-resistance model

Similar observations of the MR of Fe_3O_4 grown on MgO [27] and $SrTiO_3$ [120] have been reported. Ziese [27] modelled the MR by considering two ferromagnetic chains (with fixed spin orientation) coupled through one spin at the boundary that is allowed to change its orientation. Our model takes the full field dependence of all spins in the chain into account, including the AF coupling and thus gives a more realistic picture of the spin configuration near the boundary.

For the films grown on $SrTiO_3$ [120] the MR data show a similar field dependence as has been observed in the manganites. The transport properties of the manganites are in many respects similar to those of Fe_3O_4. Whereas the Colossal Magneto-Resistance (CMR) in the manganites is associated with the field dependence of the metal-insulator transition taking place at T_C, our results on Fe_3O_4 are related to the MR behaviour of the manganites below T_C. For the manganites, it was shown that a dominant MR-term can be generated by introducing many grain boundaries, i.e. in powdered, sintered samples. Spin-polarized tunneling between anti-ferromagnetically oriented grains is the dominant term for MR at low fields [121]. For these polycrystalline samples, the high field MR is also independent of temperature and mainly linear in the applied magnetic field and is associated with the alignment of spins in a magnetically disordered region [121, 122]. We think that this mesoscopic description of the conduction mechanism between different grains is in several respects analogous to the localized hopping model presented by us. However, in contrast to the grain boundaries, our films consist of domains that are structurally intergrown, and the magnetic properties of adjacent domains are strongly coupled. Therefore, an atomically sharp interface without a disordered region with switchable magnetic orientations is obtained.

7.5 Temperature dependence of the MR

The model described in §7.3.1 and §7.3.2 is independent of temperature. This results from the field dependent part of the conductivity, which is a single boundary property and independent of temperature. The magnitude of the magneto-resistance increases with decreasing temperature and is most likely related to the increase in spin-polarisation with decreasing temperature. To study the influence of temperature on the shape of the MR-curves, we have plotted the normalised MR in Fig. 7.5. These curves have been obtained by taking the value at 5 Tesla to be -1.
The shape of the 12 nm thick film is independent of temperature, as shown in Fig. 7.5a. This is not the case for the shape of the 30 nm thick film (Fig. 7.5b, for which the shape is more linear at 60 K. The Verwey transition of these films has been determined from resistance versus temperature measurements. The 12 nm thick film does not show a Verwey transition in the temperature range 50-300 K. The 30 nm thick film has a Verwey transition region between 95 and 105 K. The fact that the 30 nm thick film is below T_V at 60 K might explain the difference in the shape of the MR curves, even though the model holds both below and above T_V. The total conductivity is in both cases proportional to $t_0^2 cos^2\varphi$. In Fe_3O_4, both band and hopping conductivity have to be considered [21]. At lower tem-

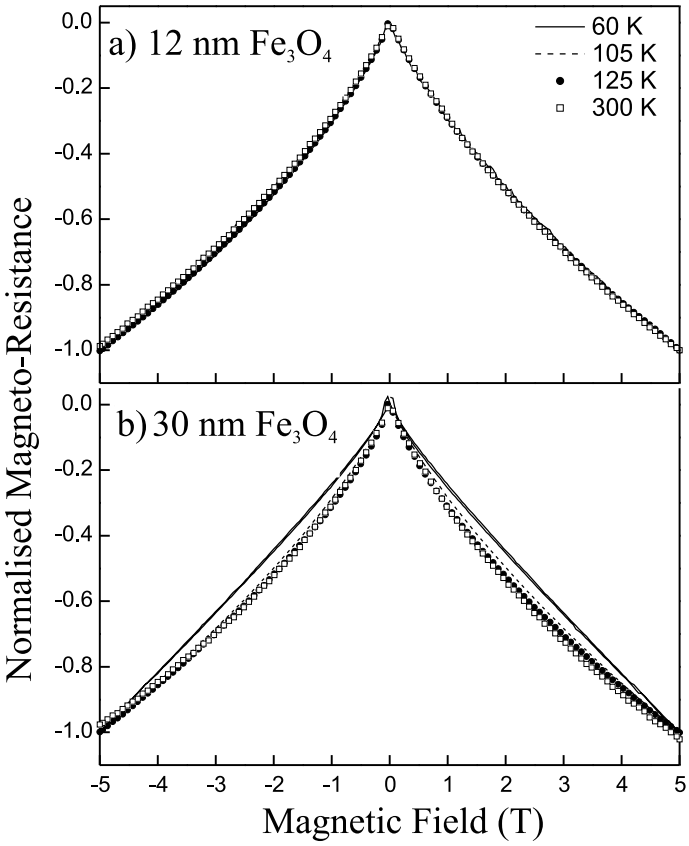

Figure 7.5: *Normalised magneto-resistances for a) 12 nm Fe_3O_4 film and b) 30 nm Fe_3O_4 film, both at 60, 105, 125 and 300 K and the magnetic field applied parallel to the film.*

peratures, where short range ordering is significant, hopping conductivity is small compared to the band conductivity. At higher temperatures hopping conductivity becomes more important due to a gradual decrease of short range ordering [21].
Both single crystals [123] and epitaxial Fe_3O_4 films [109] exhibit a peak in the MR at the Verwey transition. The 30 nm thick film also shows a peak in the MR behaviour at 100 K (MR = -16%), but only for fields applied parallel to the film plane. There is a large difference between parallel and perpendicular applied fields at this temperature. This is shown in Fig. 7.6, where the MR is plotted for the 30 nm thick film at 125, 100 and 60 K.
The large difference in parallel and perpendicular MR at 100 K is remarkable. In our model, only uniaxial out-of-plane anisotropy has been taken into account, because the value of the out-of-plane anisotropy (shape anisotropy) constant K_u (0.13 MJ/m^3) is much larger than the in plane magneto crystalline anisotropy constant K_1 (9.4 kJ/m^3). However, K_1 changes sign

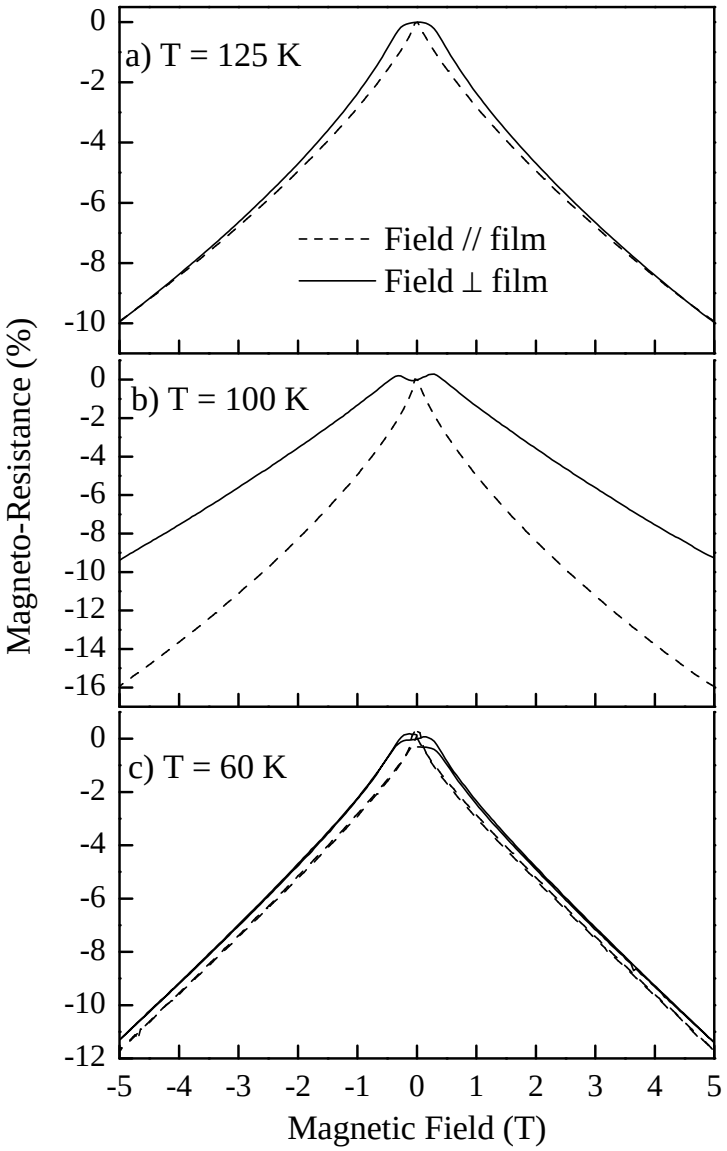

Figure 7.6: *Magneto-resistance for the 30 nm thick Fe_3O_4 film at a) 125 K, b) 100 K and c) 60 K with the magnetic field applied perpendicular (solid line) and parallel (dashed line) to the film.*

below T_V and at T_V it crosses zero, whereas the out-of-plane anisotropy is only partly reduced [119]. This will further be discussed in the next paragraph.

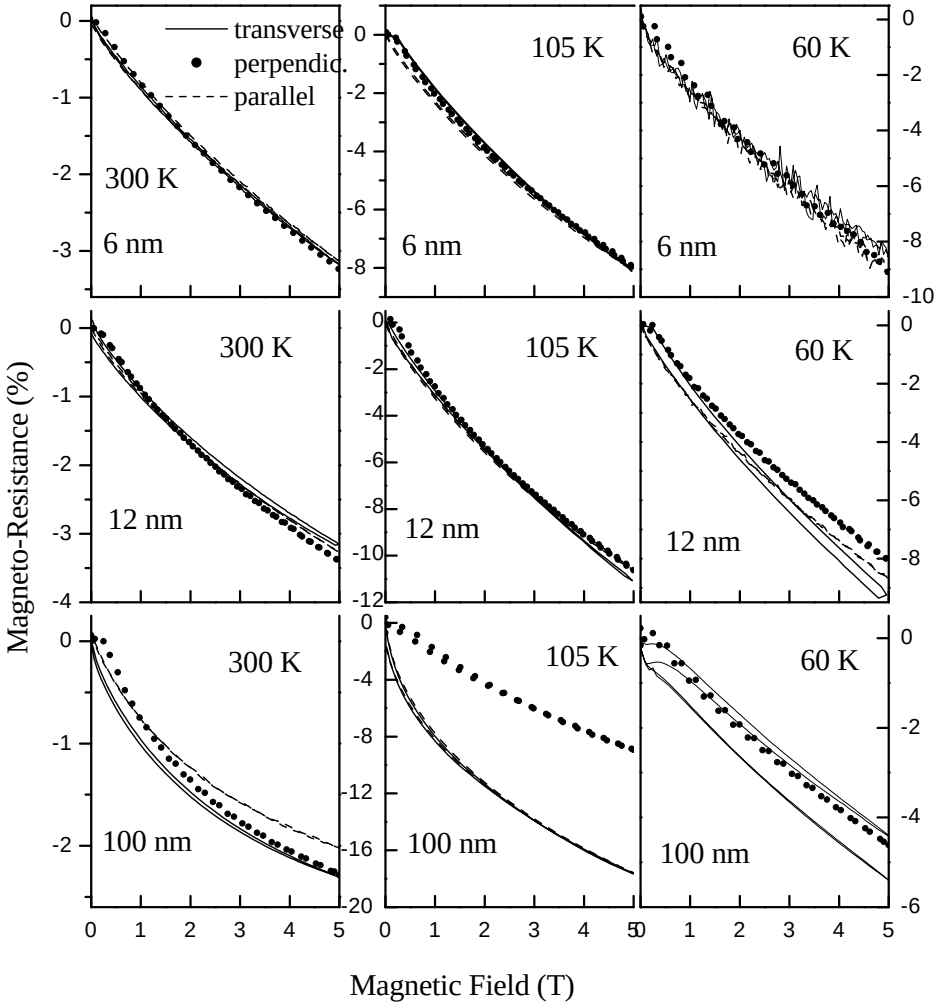

Figure 7.7: *Magneto-resistance for 6, 12 and 100 nm thick Fe_3O_4 film at 300 K, 105 K and 60 K, with the magnetic field applied perpendicular (perpend. geometry, dots) to the film and parallel to the film and current (parallel geometry, dashed line) and parallel to the film, but perpendicular to the current (transverse geometry, solid line).*

7.6 Geometry dependence of the MR

The magneto-resistance measurements have been performed with the current along the [100] direction. We have used three different geometries. In the perpendicular geometry the field was applied perpendicular to the film. In the parallel geometry, the field was applied parallel to the plane of the film and to the current and in the transverse geometry the field was applied parallel to the plane of the film and perpendicular to the current.
The magneto-resistance curves for all three geometries and for three different film thicknesses (6, 12 and 100 nm) are shown in Fig. 7.7. The measure-

ments were performed at room temperature, around the Verwey transition temperature (105 K) and at 60 K, as indicated in the figure.

For the 100 nm thick film, at room temperature the perpendicular MR is larger than the parallel MR, this is reversed at 60 K. This only occurs for the thick film that shows a Verwey transition and was also observed by Ziese [27]. The reason for this behaviour is not clear. Even though the magneto-crystalline anisotropy constant K_1 changes sign at T_v, the difference between perpendicular and parallel MR is related to out-of-plane anisotropy. The uniaxial anisotropy constant K_u is reduced below T_v, but as discussed in the previous paragraph, this difference can also be related to the band and hopping conductivity at different temperatures.
The parallel and transverse magneto-resistance would expected to be equal, but is also thickness and temperature dependent. The magnetocrystalline anisotropy constant K_1 becomes zero at T_v, after which it changes sign and the easy axis becomes $\langle 100 \rangle$ if the magnetic field is applied along this direction. For the 100 nm thick film, the parallel and transverse MR curves are indeed the same at the Verwey transition (105 K), but not at other temperatures. Very thin films, below 5 nm, have no anisotropy at all and for a 6 nm thick film the anisotropy is strongly reduced with respect to the bulk. This is apparent in the MR curves, as there is hardly any difference between the parallel and transverse geometry for this thickness.

7.7 Conclusions

We have performed magneto-resistance measurements on Fe_3O_4 films containing atomically sharp anti-ferromagnetic boundaries. The MR curves can be described by a model of spin-polarized transport across an atomically sharp AF coupled boundary. The MR measurements yield linear and quadratic field dependence up to the anisotropy field for fields applied parallel and perpendicular to the film plane respectively, in agreement with the model. The measurements have been performed over many AF boundaries. In order to fully compare the MR data with the model it is of interest to study the MR of a single boundary, as the MR is expected to be very large. For applied fields larger than the anisotropy field (0.5 T), the MR curves are expected to have a similar slope for parallel and perpendicular applied fields. At 60 K, similar slopes for both curves are observed above 0.5 Tesla. At 105 and 125 K the two curves coincide for applied fields larger than 2 Tesla. Above the Verwey transition the shape of the MR curves is independent of temperature. Below the Verwey transition, the shape becomes more linear with decreasing temperature. At the Verwey transition a large difference in MR has been observed for fields applied parallel (-16%) and perpendicular (-9.5%) to the film plane.